letters to nature

functional groups into their structures, for example phenethyl, cyclohexenyl, aminopropyl (information regarding zeolite NaY with tethered cyclohexenylethyl groups is included in Supplementary information). Additionally, we have demonstrated not only acid catalysis, but base-catalysed conversions. Finally, the organic moieties may perform functions other than catalysis, for example, synthesis of vicinal diols through oxidation of tethered cyclohexenyl groups could be used as a chelating site for adsorbing metal ions from solution. We believe that this synthetic method should be a general method for high-silica molecular sieve syntheses, and particularly syntheses mediated by F^{-}, so long as the SDA is extractable and there exists sufficient intracrystalline space for both the organic functional group and the SDA. Thus, organic-functionalized molecular sieves should provide for new applications of shape-selectivity.

Methods

Catalytic reactions. For Table 1. Reactions were conducted in magnetically stirred glass reactors at 70 °C for 24 h. The reactor was charged with 9 g toluene, 10 mmol of each reactant, and about 10 mg catalyst. Products were identified by gas chromatography using authentic samples.

For Figure 3. Reactions were conducted in magnetically stirred glass reactors at 70 °C. The reactor was charged with 10 g toluene, 10 mmol of reactants in the case of HEX or 3 mmol in the case of PYC, and 13 mg catalyst. Samples were taken periodically and analysed by GC/MS spectroscopy. Acid content of catalyst: ~0.14 mmol H^{+} g^{-1} catalyst.

Active site density. Beta/PETMS/SO$_3$H (0.21 g) was washed with 15 ml saturated NaCl solution at room temperature. The OFMS was removed by filtration. Several drops of phenolphthalein solution were added to the filtrate and then this solution was titrated with 0.001 M NaOH to neutrality. The active-site density obtained from this method agreed well with the total mass of organic material as determined by TGA, and elemental analysis for sodium.

1. Venuto, P. N. Organic catalysis over zeolites: a perspective on reaction paths within micropores. *Microporous Mater.* **2,** 297–411 (1994).
2. Tatsumi, T., Yanagisawa, K., Asano, K., Nakamura, M. & Tominaga, H. in *Studies in Surface Science and Catalysis 83* (eds Hattori, T. *et al.*) 417–424 (Elsevier, Amsterdam, 1994).
3. Kresge, C. T., Leonowicz, M. E., Roth, W. J., Vartuli, J. C. & Beck, J. S. Ordered mesoporous molecular sieves synthesized by a liquid-crystal template mechanism. *Nature* **359,** 710–712 (1992).
4. Corma, A., Iglesias, M., del Pino, C. & Sanchez, F. New rhodium complexes anchored on modified USY zeolites. *J. Chem. Soc. Chem. Commun.* 1253–1255 (1991).
5. Brunel, D., Cauvel, A., Fajula, F. & DiRenzo, F. in *Studies in Surface Science and Catalysis 97* (eds Bonneviot, L. *et al.*) 173–180 (Elsevier, Amsterdam, 1995).
6. Diaz, J. J., Balkus, K. J. Jr, Bedioui, F., Kurshev, V. & Kevan, L. Synthesis and characterization of cobalt-complex functionalized MCM-41. *Chem. Mater.* **9,** 61–67 (1997).
7. Burkett, S. L., Sims, S. D. & Mann, S. Synthesis of hybrid inorganic-organic mesoporous silica by co-condensation of siloxane and organosiloxane precursors. *Chem. Commun.* 1367–1368 (1996).
8. Lim, M. H., Blanford, C. F. & Stein, A. Synthesis and characterization of a reactive vinyl-functionalized MCM-41: probing the internal pore structure by a bromination reaction. *J. Am. Chem. Soc.* **119,** 4090–4091 (1997).
9. Fowler, C. E., Burkett, S. L. & Mann, S. Synthesis and characterization of ordered organo-silica-surfactant mesophases with functionalized MCM-41-type architecture. *Chem. Commun.* 1769–1770 (1997).
10. Macquarrie, D. J. Direct preparation of organically modified MCM-type materials: preparation and characterization of aminopropyl-MCM and 2-cyanoethyl-MCM. *Chem. Commun.* 1961–1962 (1996).
11. Lim, M. H., Blanford, C. F. & Stein, A. Synthesis of ordered microporous silicates with organo sulfur surface groups and their applications as solid acid catalysts, *Chem. Mater.* **10,** 467–470 (1998).
12. Itoh, A. & Masaki, Y. Synthesis and application of new phenyl-functionalized zeolites as protection against radical bromination at the benzylic position. *Syn. Lett.* **12,** 1450–1452 (1997).
13. Cauvel, A., Brunel, D., DiRenzo, F., Moreau, P. & Fajula, F. in *Studies in Surface Science and Catalysis 94* (eds Beyer, H. K. *et al.*) 286–293 (Elsevier, Amsterdam, 1995).
14. Li, H. X., Camblor, M. A. & Davis, M. E. Synthesis of zeolites using organosilicon compounds as structure-directing agents. *Microporous Mater.* **3,** 117–121 (1994).
15. Calabro, D. C. *US Patent 5,194,410* (1993).
16. Camblor, M. A., Corma, A. & Valencia, S. Spontaneous nucleation and growth of pure silica zeolite beta free of connectivity defects. *Chem. Commun.* 2365–2366 (1996).
17. Sudholter, E. J. R., Huis, R., Hays, G. R. & Alma, N. C. M. Solid state silicon-29 and carbon-13 NMR spectroscopy using cross-polarization and magic-angle spinning techniques to characterize 3-chloropropyl and 3-aminopropyl-modified silica gels. *J. Coll. I. Sci.* **103,** 554–560 (1985).
18. Bein, T., Carver, R. F., Farlee, R. E. & Stucky, G. D. Solid-state ^{29}Si NMR and infrared studies of the reactions of mono and polyfunctional silanes with zeolite Y surfaces. *J. Am. Chem. Soc.* **10,** 4546–4553 (1988).

Correlation between Arabian Sea and Greenland climate oscillations of the past 110,000 years

Hartmut Schulz*, Ulrich von Rad* & Helmut Erlenkeuser†

* Bundesanstalt für Geowissenschaften und Rohstoffe (BGR), PF 510153, D-30631 Hannover, Germany
† Leibniz-Labor für Altersbestimmung und Isotopenforschung, Universität Kiel, Max-Eyth-Strasse 11-13, D-24118 Kiel, Germany

Palaeoclimate studies have revealed the general high-frequency instability of Late Pleistocene climate—for example, the so-called Dansgaard–Oeschger and Heinrich events—on timescales of a few millennia, centuries or even decades[1–11]. Here we present evidence for a general relationship between low-latitude monsoonal climate variability and the rapid temperature fluctuations of high northern latitudes that are recorded in the Greenland ice records. Sediment cores from the northeastern Arabian Sea show laminated, organic-carbon-rich bands, reflecting strong monsoon-induced biological productivity, that correlate with the mild interstadial climate events in the northern North Atlantic region. In contrast, periods of lowered southwest monsoonal intensity, indicated by bioturbated, organic-carbon-poor bands, are associated with intervals of high-latitude atmospheric cooling and the injection of melt water into the North Atlantic basin. Our records suggest that Dansgaard–Oeschger and Heinrich events are strongly expressed in low-latitude (monsoonal) climate variability, suggesting the importance of common forcing agents such as atmospheric moisture and other greenhouse gases.

Today, the northern Arabian Sea is characterized by (1) warm and highly saline near-surface waters originating from the Persian Gulf,
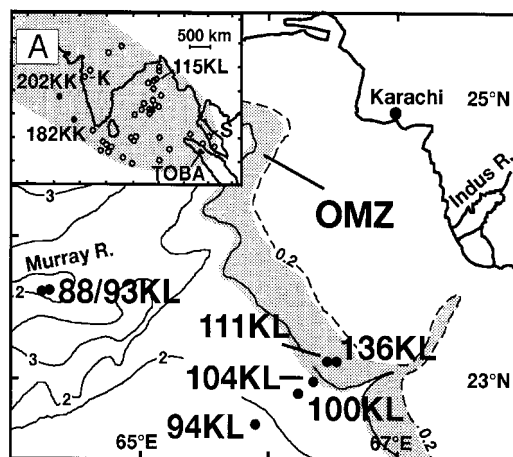

Figure 1 Location of sediment cores off Pakistan. OMZ, oxygen-minimum zone impinging on the continental slope between 200 and 1,200 m water depth (w.d.) with contours in km. Labelled sites and key cores SO90-88KL and SO90-93KL (23° 35′ E, 64° 13′ E, 1,783 m and 1,802 m w.d.), SO90-111KL (23° 06′ N, 66° 29′ E, 775 m w.d.), SO90-136KL (23° 07′ N, 66° 30′ E, 568 m w.d.) are discussed in the text. Inset map showing sites of youngest Toba ash occurrences between Toba (Sumatra) and the northeastern Arabian Sea. 'A' indicates position of main map. Open circles, localities from the Bay of Bengal, India (K indicates Kukdi) and southern Malaysia (S indicates Serdang)[23–25] (H. R. Kudrass, personal communication); filled circles: Arabian Sea IIOE cores[12].

(2) high fluxes of both wind- and river-transported (Indus) terrestrial sediment, and (3) high oceanic (monsoonal) surface-water productivity and biogenic fluxes, leading to (4) a stable, mid-depth oxygen-minimum zone (OMZ) at 200–1200 m water depth (Fig. 1). The OMZ prevents bioturbation and favours the accumulation of organic-carbon-rich, partly laminated or even varved sediments[12] (here we will use TOC to denote total organic carbon). These conditions offer a unique opportunity to study in detail the variability of the tropical monsoonal circulation and marine productivity on millennial to annual timescales during the last glacial–interglacial cycle[13]. In contrast to the northwestern Arabian Sea where a seasonal reversal in surface circulation occurs due to the strong summer southwestern-monsoon winds (July–August) and (less intense) northeastern winds during winter (December–February), the seasonal variation of current directions is less distinct off Pakistan. Although geochemical analyses show that the organic matter fraction is predominantly of marine origin, the stable oxygen isotopes of planktonic foraminifera in the surface sediments do not show a clear upwelling signal of cool subsurface waters. We infer that the seasonal productivity in the northeastern Arabian Sea is temporally and spatially linked to the strong coastal and open-ocean

upwelling cells off Oman by the lateral advection of nutrient-rich waters from the southwest due to the anticyclonic surface gyre during the summer months[14].

The sediment cores taken from OMZ water depths along the continental margin off Pakistan (Fig. 1) reveal a consistent pattern of dark, TOC-rich, partly laminated intervals alternating with light-coloured, TOC-poor, pteropod-rich, bioturbated intervals (Fig. 2). TOC concentrations in the hemipelagic sediments of cores SO90-88/93KL from the Murray ridge below the present OMZ are generally much lower, and show significant variability only on the longer-term, orbitally induced timescales. However, these cores also document nearly identical high-frequency variability, seen in distinct peaks of pteropod debris and increased biogenic sand content corresponding to the bioturbated, pteropod-rich and TOC-poor intervals in the OMZ cores. Here we use the record of sonic velocity (V_p) reflecting the bulk compositional changes in the sediment. Based on geochemical and micropalaeontological investigations and on the spatial distribution of laminated sediments from box core tops from this area[13], we suggest that the multiple facies changes in our cores reflect fluctuations in the intensity of summer monsoonal productivity. Apparently, the oxygenation of
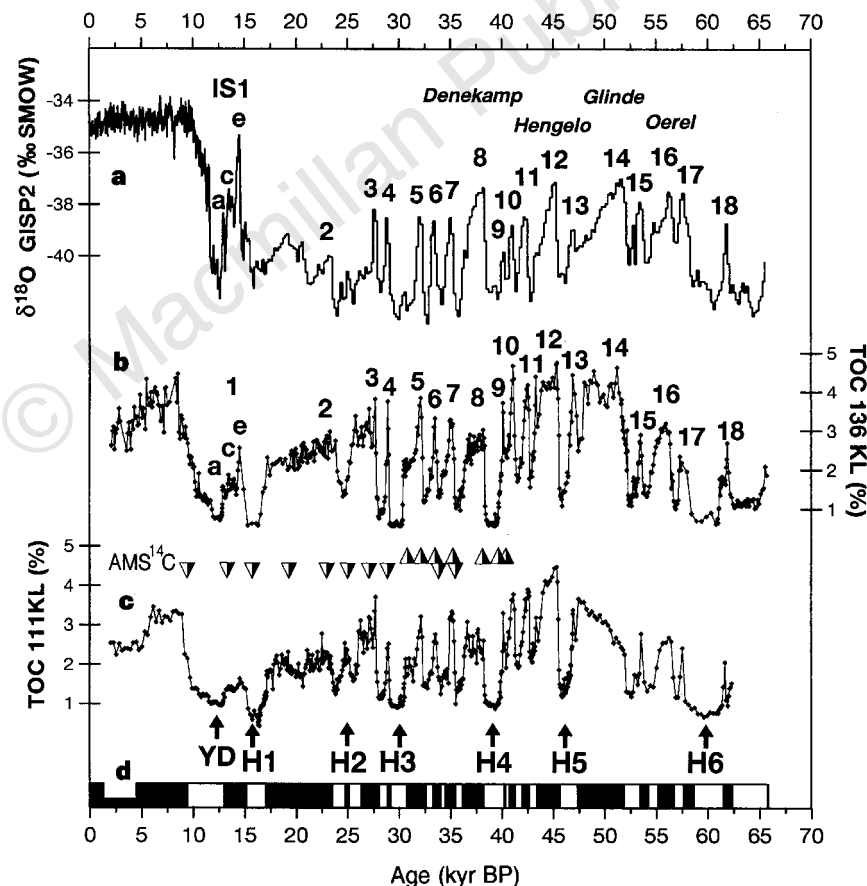

Figure 2 Correlation of high-frequency climate variability for the past 65,000 years between ice-core and marine-sediment-core records. **a**, Greenland GISP2 $\delta^{18}O_{ice}$ record[1]; **b** and **c**, two high-resolution (average sample resolution ~100 yr) marine TOC-records of cores SO90-111KL and SO90-136KL off Pakistan, based on a 1:1 fit using the GISP2 chronology. Following the generalized lithology shown in **d**, profiles from the centre of the OMZ are characterized by conspicuous alternations between dark-coloured, distinctly to indistinctly laminated, TOC-rich (black in **d**) and light-coloured, bioturbated pteropod-rich and TOC-poor intervals (white in **d**), indicating millennial- to centennial-scale variability of monsoonal surface water productivity and bottom-water oxygenation. Numbers indicate Greenland interstadials IS1–18, and equivalent Arabian Sea monsoonal events 1–18; H1–H6 indicate northern North Atlantic Heinrich meltwater events, coinciding with the

deposition of bioturbated intervals in the Arabian Sea record. YD, Younger Dryas; triangles in **b** and **c** show AMS ^{14}C dates. Total organic carbon (TOC, as percentage of dry weight) contents were calculated from sediment colour (grey-scale) measurements. Based on 138 and 136 paired samples, polynomial regression equations revealed $r^2 = 0.93$ and $s = 0.35\%$ for cores 111KL and 136KL/137KA[13], respectively. For AMS dating, monospecific samples of planktic foraminiferal species were mostly taken from the laminated sections where biases due to bioturbational mixing can be ruled out. Radiocarbon ages were calibrated to a calendar timescale[29] (except for the youngest sample[30]), after a correction of –640 yr for the local marine reservoir effect determined from varved surface sediments. These data are available; see Supplementary information.

bottom waters is directly influenced by these fluctuations resulting in strong variations of the intensity of the OMZ during the last glacial period.

Our records from the OMZ off Pakistan show striking similarities with the record of $\delta^{18}O$ from the Greenland GRIP and GISP2 ice cores that documents extremely rapid fluctuations in air temperature in the high northern latitudes during the last glacial–interglacial cycle[1,2]. Generally, the light-coloured, bioturbated intervals correspond to periods of extremely 'light' (^{18}O-depleted) $\delta^{18}O$ values in the GISP2 ice core indicating cool air temperatures over Greenland and the northern North Atlantic Ocean (Fig. 2). This applies particularly for the six intervals of bioturbated, $CaCO_3$- and pteropod-rich sediments in the OMZ cores which can be correlated to the Younger Dryas cool period at around 12,600 years BP and to the Heinrich events H1–H6 of ice-rafted detritus that were associated with massive discharges of melt water into the North Atlantic[3,4]. Conversely, the dark-coloured, indistinctly to distinctly laminated intervals in the Arabian Sea sediments appear as equivalents to all Greenland Dansgaard–Oeschger interstadials IS1 to IS18. Similar to the Greenland ice record, there is a clear pattern of two intervals of prominent triple peaks of high organic carbon content, IS5, IS6, IS7, and IS9, IS10, IS11. Both triple peaks are preceded by broader events corresponding to IS8 (Denekamp) and IS12 (Hengelo). For the early marine oxygen isotope stage 3, stage 4

and the late stage 5 (Figs 2 and 3), bundles of intervals can be grouped as equivalents to events IS13, IS14 (Glinde), IS15, IS16, IS17 (Oerel), to IS21 (Odderade), and to IS22, IS23, IS24 (Brørup) according to the nomenclature of the northwest European interstadial periods[1]. The Atlantic-type structure of the Bølling/Allerød climate interval (IS1, a, c, e) consisting of three 'cool' and four 'warm' episodes[15] is also recorded.

High-frequency monsoonal variability in the properties of surface waters is also documented in the stable-isotope record of the near-surface-dwelling foraminiferal species *Globigerinoides ruber* (Fig. 3b). The glacial to interglacial $\delta^{18}O$ amplitude is ~2‰. The global ice-volume effects of ~1.3‰ leaves up to 0.7‰ to be explained by the local variability of water temperature of the order of ±3–4°C and/or salinity of ±1–1.5‰. We observe a strong long-term fluctuation in our record on the 23,000-year precessional cycle of solar radiation, forcing the monsoons[16], as broad $\delta^{18}O$ maxima are centred around 20,000, 42,000, 64,000 and 87,000 yr BP. For instance, the broad mid-stage-3 maximum at 42,000 yr BP is of regional significance and is not seen in the standard marine $\delta^{18}O$ record that is used for global chronostratigraphic correlation[17]. Superimposed, further distinct millennial- to centennial-scale $\delta^{18}O$ maxima indicate periods of high surface salinity and/or lowered temperature that are associated with the equivalents of the Heinrich events seen in the V_p-record. Conversely, nearly all
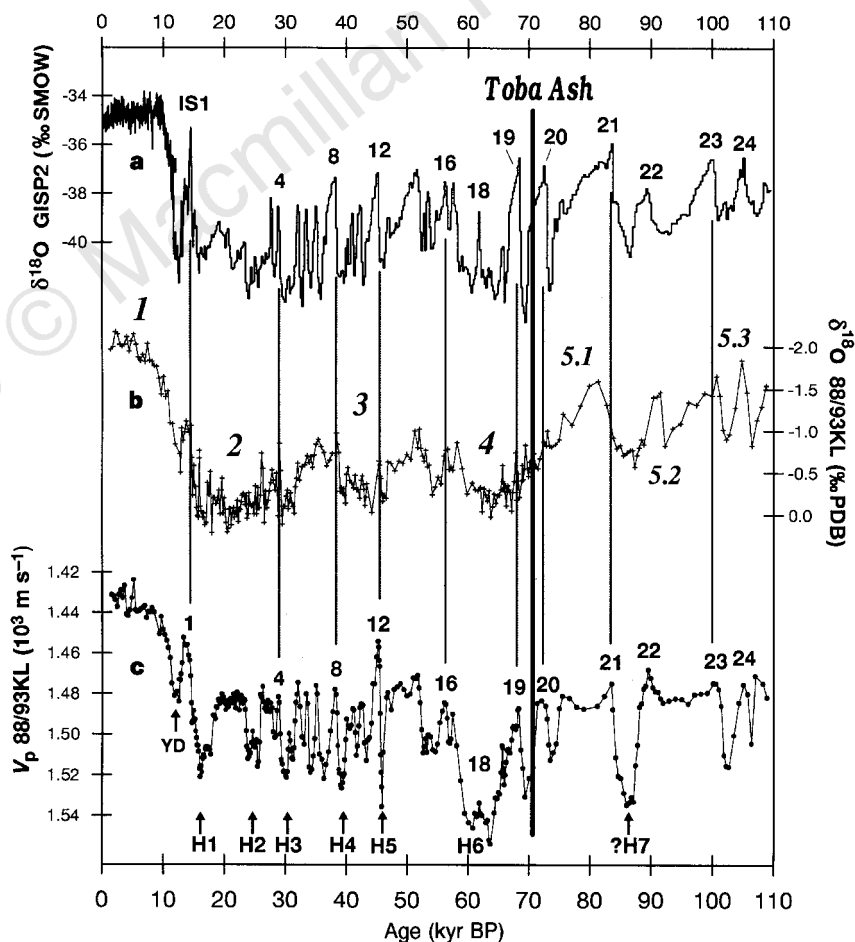

Figure 3 Correlation of high-frequency climate variability for the past 110,000 yr between ice-core and marine-sediment-core records. **a**, Greenland GISP2 $\delta^{18}O_{ice}$ record; **b**, the marine $\delta^{18}O$ stable-isotope record of the planktic foraminifer *Globigerinoides ruber*; **c**, the record of sonic velocity (V_p) of sediment cores SO90-88/93KL. Notation of interstadials IS1–IS24, YD, Heinrich events H1–H7 and Arabian Sea equivalent events 1–24 follows Fig. 2. Italic numbers *1–5.3* indicate

standard SPECMAP[17] oxygen-isotope stages. In cores 88KL and 93KL, shards derived from the Toba mega-eruption occur at 620–624 and 623–627 cm core depth, respectively, near the isotope stage 4/5 boundary, that is, between Greenland interstadials IS19 and IS20 as well as between Arabian Sea equivalents 19 and 20.

interstadial equivalents seem to be related with minima in the $\delta^{18}O$ record. A series of similar century-scale $\delta^{18}O$-events at the glacial/interglacial transition is reported from the northwestern Arabian Sea, suggesting that the onset and intensification of southwest-monsoonal circulation and surface water productivity occurred at discrete steps at the end of the last glaciation[18], in phase with the onset and subsequent events of deglacial warming in the high latitudes[19].

Confirmed by evidence from seventeen AMS-radiocarbon ages and high-resolution stable-isotope stratigraphy we suggest that our sediment cores show for the past 110,000 years a record of low-latitude monsoonal variability to be correlated to the cool Younger Dryas and Heinrich events H1–H7, and to the interglacial/interstadial Holocene, Bølling/Allerød and Dansgaard–Oeschger IS1–IS24 climate intervals, respectively, seen in the Greenland temperature record.

Our correlations are further supported by the identification of the youngest Toba ash horizon in the Arabian Sea sediments, also manifested as a distinct aerosol peak in the Greenland GISP2 ice core ~71,000 years ago, between interstadials IS19 and IS20[20]. The Toba eruption, the largest Quaternary volcanic eruption on Earth, produced more than $800\,km^3$ of rhyolitic bubble-wall shards and pumice which were deposited during a few weeks covering at least 1% of the Earth's surface with an extensive ash blanket[21,22]. Owing to the prevailing tropospheric jet streams, the youngest Toba ash was mainly dispersed to the west-northwest. Up to now particles have been traced from Malaysia to the Bay of Bengal up to western India, ~3,100 km from the source[23–25] (Fig. 1). By careful inspection of our records from the International Indian Ocean Expedition and off Pakistan[12,13,14], the youngest Toba ash was identified in the Arabian Sea cores IIOE-182KK and −202KK, in SO90-94KL, −100KL and −104KL from the upper Indus fan, and in cores SO90-88 and −93KL from the northeastern Murray ridge. These sites extend the maximum distance of the Toba ash occurrences to more than 4,000 km from the source and the area of the ash blanket to $> 4 \times 10^6\,km^2$.

We investigated the composition of the volcanic particles in Arabian Sea core SO90-94KL where a disseminated (bioturbated) ash was found at 520 cm core depth consisting of fresh, transparent bubble-wall shards and in Bengal fan core SO93-115KL (Fig. 1) from a discrete 6-cm-thick ash layer (H. R. Kudrass, personal communication). The chemical composition was determined by analysing discrete glass shards by electron microprobe. The Arabian Sea results show very similar major-element contents to the Bengal fan samples, and correlate well with the composition from the distal Bengal fan, western India, ODP Site 758 on the outermost Bengal fan, as well as the most proximal ash at Malaysia. The chemical results on the youngest Toba ash composition correlated from Sumatra to the Arabian Sea are available (see Supplementary Information).

In cores SO90-88/93KL, rhyolithic shards occur at narrow intervals of a few centimetres near the boundary between marine isotope stages 4 and 5 (Fig. 3), in a similar position to the records from the Bay of Bengal[23]. As cores SO90-88/93KL are situated in an isolated position on the Murray ridge, we can exclude downslope reworking. We suggest that the glass shards were rapidly deposited as fallout ash and then slightly disseminated due to bioturbational mixing. Based on $\delta^{18}O$ stratigraphy we estimate ages of ~72,400 to $74,600 \pm 5,000$ yr BP for the Toba ash in the Arabian Sea cores, in good agreement with the ages centred at $74,000 \pm 2,000$ yr BP based on K/Ar, $^{40}Ar/^{39}Ar$, and fission trackdating of glass shards from terrestrial outcrops[23,24]. In contrast, the SO_4^{2-} peak attributed to the Toba mega-eruption in the GISP2 core from Greenland has been attributed a slightly younger age of ~71,100 ± 5,000 yr BP, using the correlated age model from the two $\delta^{18}O_{ice}$-records of GISP2 and Vostok[26]. However, the Toba ash as an isochronous stratigraphic horizon directly correlates the Arabian Sea and Greenland records

far beyond the reach of radiocarbon dating (Fig. 3). In the GISP2-record the Toba signal is placed at the late IS20; in cores SO90-88/93KL the Toba ash occurs between the equivalent monsoonal events 19 and 20.

Our records from the northwestern Indian Ocean suggest that the rapid Dansgaard–Oeschger- and Heinrich-style events known from Greenland and the northern North Atlantic are a significant component also of low-latitude climate variability during the past 110,000 years, due to millennial to centennial fluctuations in the intensity of southwest monsoonal circulation. These rapid fluctuations point to large-scale climate elements in the ocean–atmosphere system interacting rapidly in the high and low latitudes. We suggest that the record of mild interstadials found in the Greenland ice cores reflect periods of global warmth, associated with high levels of tropospheric moisture and other greenhouse gases[27,28]. □

1. Dansgaard, W. et al. Evidence for general instability of past climate from a 250-kyr ice-core record. Nature **364**, 218–220 (1993).
2. Johnsen, S. J. et al. Irregular glacial interstadials recorded in a new Greenland ice core. Nature **359**, 311–313 (1992).
3. Broecker, W., Bond, G., Klas, M., Clark, E. & McManus, J. Origin of the northern Atlantic Heinrich events. Clim. Dyn. **6**, 265–273 (1992).
4. Grousset, F. et al. Patterns of ice-rafted detritus in the glacial North Atlantic. Paleoceanography **8**, 175–192 (1993).
5. Kotilainen, A. & Shackleton, N. J. Rapid climate variability in the North Pacific Ocean during the past 95,000 years. Nature **377**, 323–326 (1995).
6. Tada, R., Irino, T. & Koizumi, I. in Proc. of the 1994 Sapporo IGBP Symp., Global Fluxes of Carbon and Its Related Substances in the Coastal Sea-Ocean-Atmosphere System (ed. Tsunogai, S.) 517–522 (Sapporo, 1995).
7. Porter, S. C. & An, Z. S. Correlation between climate events in the North Atlantic and China during the last glaciation. Nature **375**, 305–308 (1995).
8. Behl, R. J. & Kennett, J. P. Brief interstadial events in the Santa Barbara basin, NE Pacific during the past 60 kyr. Nature **379**, 243–246 (1996).
9. Mayewski, P. A. et al. Climate change during the Last Deglaciation in Antarctica. Science **272**, 1636–1638 (1996).
10. Bender, M. et al. Climate correlations between Greenland and Antarctic during the past 100,000 years. Nature **372**, 663–666 (1994).
11. Jouzel, J. Ice cores north and south. Nature **372**, 612–613 (1994).
12. von Stackelberg, U. Faziesverteilung in Sedimenten des indisch-pakistanischen Kontinentalrandes (Arabisches Meer). "Meteor"-Forsch.-Ergebn., Reihe C **9**, 1–73 (1972).
13. von Rad, U., Schulz, H. & SONNE 90 Scientific Party Sampling the oxygen minimum zone off Pakistan: glacial/interglacial variations of anoxia and productivity. Mar. Geol. **125**, 7–19 (1995).
14. Schulz, H., von Rad, U. & von Stackelberg, U. in Paleoclimatology and Paleoceanography from Laminated Sediments (ed. Kemp, A. E. S.) 185–207 (Geol. Soc. Spec. Publ. No. 116, Blackwell Scientific, Oxford, 1996).
15. Hughen, K., Overpeck, J. T., Peterson, L. C. & Trumbore, S. Rapid climate changes in the tropical Atlantic region during the last deglaciation. Nature **380**, 51–54 (1996).
16. Clemens, S., Prell, W., Murray, D., Shimmield, G. & Weedon, G. Forcing mechanisms of the Indian ocean monsoon. Nature **353**, 720–725 (1991).
17. Martinson, D. G. et al. Age dating and the orbital theory of the ice ages: development of a high-resolution 0 to 300,000 year chronostratigraphy. Quat. Res. **27**, 1–29 (1987).
18. Sirocko, F. et al. Century-scale events in monsoonal climate over the past 24,000 years. Nature **364**, 322–324 (1993).
19. Sirocko, F., Garbe-Schönberg, D., McIntyre, A. & Molfino, B. Teleconnections between the subtropical monsoons and high-latitude climates during the last deglaciation. Science **272**, 526–529 (1996).
20. Zielinski, G. A. et al. Potential atmospheric impact of the Toba mega-eruption 71,000 years ago. Geophys. Res. Lett. **23**, 837–840 (1996).
21. Rose, W. I. & Chesner, C. A. Dispersal of ash in the great Toba eruption, 75 ka. Geology **15**, 913–917 (1987).
22. Rose, W. I. & Chesner, C. A. Worldwide dispersal of ash and gases from earth's largest known eruption: Toba, Sumatra, 75 ka. Palaeogeogr. Palaeoclimatol. Palaeoecol. **89**, 269–275 (1990).
23. Ninkovich, D., Shackleton, N. J., Abdel-Monem, A. A., Obradovich, J. D. & Izett, G. K-Ar age of the Pleistocene eruption of Toba, north Sumatra. Nature **276**, 574–577 (1978).
24. Chesner, C. A., Rose, W. I., Deino, A., Drake, R. & Westgate, J. A. Eruptive history of Earth's largest Quaternary caldera (Toba, Indonesia) clarified. Geology **19**, 200–203 (1991).
25. Acharyya, S. K. & Basu, P. K. Toba ash on the Indian subcontinent and its implications for the correlation of late Pleistocene alluvium. Quat. Res. **40**, 10–19 (1993).
26. Meese, D. et al. in Preliminary Depth-age Scale of the GISP2 Ice Core (Spec. Re. 94-1, Cold Regions Research and Engineering Lab., Hanover, New Hampshire, 1994).
27. Mayewski, P. A. et al. Changes in atmospheric circulation and ocean ice cover over the North Atlantic during the last 41,000 years. Science **263**, 1747–1751 (1994).
28. Brook, E. J., Sowers, T. & Orchardo, J. Rapid variations in atmospheric methane concentration during the past 110,000 years. Science **273**, 1087–1091 (1996).
29. Bard, E., Rostek, F. & Sonzogni, C. Interhemispheric synchrony of the last deglaciation inferred from alkenone palaeothermometry. Nature **385**, 707–710 (1997).
30. Stuiver, M. & Braziunas, T. F. Modeling atmospheric ^{14}C-influences and ^{14}C ages of marine samples to 10,000 BC. Radiocarbon **35**, 137–189 (1993).